Published OnlineFirst July 17, 2017; DOI: 10.1158/1535-7163.MCT-16-0900

Molecular Cancer Therapeutics

Inhibition of Heparanase in Pediatric Brain Tumor Cells Attenuates their Proliferation, Invasive Capacity, and *In Vivo* Tumor Growth

Argyris Spyrou[1], Soumi Kundu[1], Lulu Haseeb[1], Di Yu[1], Tommie Olofsson[1], Keith Dredge[2], Edward Hammond[2], Uri Barash[3], Israel Vlodavsky[3], and Karin Forsberg-Nilsson[1]

Abstract

Curative therapy for medulloblastoma and other pediatric embryonal brain tumors has improved, but the outcome still remains poor and current treatment causes long-term complications. Malignant brain tumors infiltrate the healthy brain tissue and, thus despite resection, cells that have already migrated cause rapid tumor regrowth. Heparan sulfate proteoglycans (HSPG), major components of the extracellular matrix (ECM), modulate the activities of a variety of proteins. The major enzyme that degrades HS, heparanase (HPSE), is an important regulator of the ECM. Here, we report that the levels of HPSE in pediatric brain tumors are higher than in healthy brain tissue and that treatment of pediatric brain tumor cells with HPSE stimulated their growth. In addition, the latent, 65 kDa form of HPSE (that requires intracellular enzymatic processing for activation) enhanced cell viability and rapidly activated the ERK and AKT signaling pathways, before enzymatically active HPSE was detected. The HPSE inhibitor PG545 efficiently killed pediatric brain tumor cells, but not normal human astrocytes, and this compound also reduced tumor cell invasion *in vitro* and potently reduced the size of flank tumors *in vivo*. Our findings indicate that HPSE in malignant brain tumors affects both the tumor cells themselves and their ECM. In conclusion, HPSE plays a substantial role in childhood brain tumors, by contributing to tumor aggressiveness and thereby represents a potential therapeutic target. *Mol Cancer Ther; 16(8); 1–12. ©2017 AACR.*

Introduction

Aggressive childhood medulloblastomas and central nervous system (CNS) embryonal tumors [CNS-ET, previously referred to as supratentorial primitive neuroectodermal tumors (sPNET)] arise from undifferentiated, or poorly differentiated neural cells, which may display divergent differentiation along the neuronal and astrocytic lineages (1). Medulloblastomas originate in the cerebellum, whereas CNS-ETs develop above the tentorium and are distributed in the frontal, temporal, and parietal lobes (2). Despite certain histologic similarities, CNS-ETs are less common, but more aggressive than medulloblastomas, with a poorer survival rate (1). New classification reveals that CNS-ETs are molecularly highly heterogeneous, some sharing characteristics with already classified entities, and the remainder being distinguishable as four molecular and morphological variants (3).

Medulloblastoma and CNS-ETs are invasive, spreading to other regions of the brain and spinal cord, but more seldomly outside the CNS. Standard treatment consists of surgery, radiation, and chemotherapy, with the outcome depending on the characteristics of the tumor subgroup (1). Complete resection is often not possible and remaining tumor cells rapidly invade and form new tumors in the same or adjacent regions. Recurrence, which often occurs concomitantly with metastasis, leads to more aggressive phenotypes. Moreover, chemo-radiotherapies can render cancer cells more aggressive and invasive, for example, by activating various metalloproteases (MMP), such as MMP-9 (4). Consequently, greater understanding of the mechanisms underlying invasion by pediatric tumors, and specific effective novel therapies are required.

Invasion by cancer cells is influenced by the microenvironment, including components of the extracellular matrix (ECM) such as heparan sulfate proteoglycans (HSPG) composed of a core protein with attached HS chains and ubiquitously associated with the cell surface, as secreted entities in the ECM or in intracellular secretory vesicles. We, and others have shown that these major components of the brain ECM are altered in brain tumors (5–7). A multitude of growth factors, chemokines, and morphogens bind to HPSGs, regulating biological processes and modulating the adhesion and spread of tumor cells. Accordingly, enzymes that degrade ECM influence ligand availability and can thereby alter cell motility. Heparanase (HPSE), the main such enzyme, is an endo-β-D-glucuronidase that cleaves HS at specific sites, into 5 to 7 kDa size fragments (8) and has been correlated to the tumorigenic and metastatic capacity of several cancers and to significantly reduce postoperative survival (9–11).

Here, we show that HPSE is highly expressed in pediatric brain tumors, but low or negligible in normal brain tissue. Treatment

[1]Department of Immunology, Genetics and Pathology and Science for Life Laboratory, Uppsala University, Uppsala, Sweden. [2]Zucero Therapeutics Pty Ltd., Darra, Brisbane, Queensland, Australia. [3]Cancer and Vascular Biology Research Center, Bruce Rappaport Faculty of Medicine, Haifa, Israel.

Note: Supplementary data for this article are available at Molecular Cancer Therapeutics Online (http://mct.aacrjournals.org/).

Current address for T. Olofsson: National Board of Forensic Medicine, Uppsala, Sweden.

Corresponding Author: Karin Forsberg-Nilsson, Department of Immunology, Genetics and Pathology, Rudbeck Laboratory, Uppsala University, 75185 Uppsala, Sweden. Phone: 46-18-471-4158; Fax: 46-18-471-2000; E-mail: karin.nilsson@igp.uu.se

doi: 10.1158/1535-7163.MCT-16-0900

Published OnlineFirst July 17, 2017; DOI: 10.1158/1535-7163.MCT-16-0900

with HPSE of pediatric brain tumor cells derived from patients enhanced proliferative pathways and, conversely inhibition of HPSE suppressed tumor cell growth, migration, and invasion *in vitro*. Furthermore, blocking HPSE activity reduced proliferation of xenografted PNET and medulloblastoma with no obvious adverse side effects. We therefore conclude that inhibition of HPSE efficiently suppresses growth and dissemination of pediatric brain tumors cells.

Materials and Methods

Tissue microarrays and pediatric patient samples

Human brain tumor tissue was obtained in accordance with an ethically reviewed and approved protocol. Written informed consent was received from participants prior to inclusion in the study. Tissue microarray (TMA) analysis was performed on duplicate paraffin-embedded core samples (1 mm in diameter) from CNS-ETs (10 cases), medulloblastomas (8 cases), or normal brain tissue ($n = 8$). The slides were deparaffinized in xylene, rehydrated and boiled in epitope-retrieval buffer (DAKO). Using the autostainer 480 instrument (Lab Vision), IHC staining with rabbit anti-human HPSE antibodies (ab733) was performed overnight at 4°C with 3,3′-diaminobenzidine (DAB) as substrate. The slides were counterstained with hematoxylin and mounted. Scanning, visualization, and quantification were done using the ScanScope XT system and software (Aperio Technologies). Surgical specimens of brain tumor tissue from two CNS-ETs and two medulloblastoma cases were lysed using TissueLyser II (Qiagen) following the manufacturer's protocol. The lysates were processed further for Western blotting. Human fetal cerebellum (GTX22662; GeneTex) was used as control.

Cell culture

The supratentorial primitive neuroectodermal PNET tumor cell line (PFSK-1; ref. 2), D324 Med, and D283 Med medulloblastoma cell lines (12) were kindly provided by Prof. D. Bigner (Duke University Medical Center, Durham, NC) and Chinese Hamster Ovary cell lines, stably transfected either with a cDNA vector encoding the 50 kDa active form of HPSE or the empty vector were cultured as described previously (13). For serum starvation, the cells were maintained in medium without serum for 24 hours. Normal human primary astrocytes (3H Biomedical) were cultured on plates coated with poly-L-lysine (0.02 mg/mL) in astrocyte medium supplemented with 2% FBS, 5% penicillin/streptomycin and astrocyte growth supplement (3H Biomedical). The astrocytes were used for experiments no longer than two passages. All cell lines were tested negative for mycoplasma infection using the MycoAlert Mycoplasma Detection Kit (Lonza). For collagen invasion assay, PFSK-1 and D324 Med cells were cultured in a neural stem cell media to allow the formation of tumor spheres (14).

Western blotting and antibodies

After collection of the cells, homogenization in RIPA buffer (7), and storage on ice for 30 minutes, the cell supernatant was obtained by centrifugation at 13,000 rpm for 20 minutes at 4°C, and protein concentration measured using the BCA Kit (Roche). The protein was subjected to NuPAGE Bis-Tris on precast gels and then transferred to a nitrocellulose membrane (iBlot transfer stack; Invitrogen). For immunoblotting, the following primary antibodies were used: rabbit anti-human HPSE polyclonal ab1453 and ab733 (15), rabbit polyclonal (IgG), anti-human (LS-B2441) antibodies (LifeSpan Biosciences); antibodies against phosphorylated-p44/42 and total 44/42 MAPK (Erk1/2), phosphorylated Akt (pSer473) and total Akt, phosphorylated Src (Tyr416) and total Src, phosphorylated FAK (pTyr397) and total FAK (Cell Signaling Technology), and anti-β-actin mAb (Clone AC-15; Sigma-Aldrich). Incubation was followed by horseradish peroxidase–conjugated anti-mouse or anti-rabbit IgG (GE Healthcare).

Treatment with HPSE

For treatment with enzymatically active HPSE, conditioned medium (CM) from either CHO-HPSE or CHO-Vo cells (24-hour conditioning period) was passed through a 0.2-μm polyethersulfone (PES) syringe filter (VWR) and combined with serum-free fresh medium in a ratio of 3: 1 before adding to cell cultures. For recombinant HPSE (rHPSE) treatment, one dose of 1 μg/mL of purified 65-kDa recombinant HPSE (15, 16) was added in fresh medium, and cell counting was performed at timepoints 0, 24, and 72 hours by a Countess Automated Cell Counter (Invitrogen). To evaluate signaling pathways, fresh serum-free medium containing 1 μg/mL rHPSE was added to the cells after 24 hours of serum starvation and lysates were collected at 0, 10, and 30 minutes, and 1, 4, and 24 hours after addition of HPSE for Western blotting.

Lentiviral construction and stable transduction

Short hairpin DNA oligomers targeting HPSE (^{423}GGAATCAACCTTTGAAGAG^{441}) or nontargeting oligomers (7) were purchased from Sigma and cloned into the pBMN (CMV-G2L2P; ref. 17) vector containing reporter genes for GFP and luciferase (Luc2) and the gene for the puromycin resistance to allow selection. Lentivirus vectors, in which the expression of these genes was under control of the consecutive H1 promoter, were propagated essentially as described previously (17). A total of 100,000 cells were plated onto six-well plates, incubated for 24 hours at 37°C under 5% CO_2, placed in fresh medium containing 6 μg/mL sequabrene (polybrene-hexadimethrine bromide; SIGMA) followed by the addition of 2 to 15 μL lentiviral particles for an additional 24 hours. The medium was replaced with routine medium for 48 hours, after which medium containing 1 μg/mL puromycin was added for selection.

RNA preparation and qPCR

Total RNA was extracted using the RNeasy Mini Kit (Qiagen), in accordance with the manufacturer's protocol. cDNA was prepared employing the iScript c DNA Synthesis Kit (Bio-Rad) and the cDNA templates diluted three times for performance of qPCR reactions with SsoFast Evagreen supermixes (Bio-Rad). The levels of HPSE and HPRT-1 mRNA were quantified with the following primers: HPSE: Forward CGGCTAAGATGCTGAAGAGC Reverse TGATGCCATGTAACTGAATCAA, HPRT-1: Forward GACCAGTCAACAGGGGACAT Reverse GTCAATTATATCTTCCACAATCAAG.

Indirect immunofluorescent staining of fixed cells

Cells fixed with 4% paraformaldehyde for 15 minutes at room temperature and washed in PBS three times for 5 minutes were permeabilized and treated for 1 hour with blocking/permeabilization buffer containing 5% normal goat serum (NGS) and 0.1% to 0.3% Triton-X 100 in PBS and stained with primary rabbit anti-human HPSE (#733) antibodies overnight at 4°C. Cells were washed as above in PBS; incubated with the secondary antibody

Published OnlineFirst July 17, 2017; DOI: 10.1158/1535-7163.MCT-16-0900

Alexa Fluor 555-conjugated donkey anti-mouse IgG diluted in PBS 1:200 (Invitrogen) for 1 hour at room temperature and their nuclei stained with Hoechst 33342, trihydrochloride (1:5,000; Life Technologies) for 10 minutes. For staining of F-actin filaments, adherent cells were incubated with Alexa Fluor 568 Phalloidin diluted 1:1,000 (Life Technologies) for 1 hour at room temperature. The coverslips were mounted using fluorescent mounting medium (DAKO) and staining visualized with Zeiss AxioImager M2 fluorescence microscope (Carl Zeiss).

Effect of PG545 on tumor formation *in vivo*

PFSK-1 and D-283 Med cells (3×10^6 cells/100 μL) were injected subcutaneously into the flanks of 8- to 10-week-old NOD-SCID mice and tumor size measured 1, 7, 9, 11, 14, 16, 18, 21, and 23 days later, using a Vernier caliper. When the tumors reached a size of 100 mm^3, PG545 (18), an inhibitor of HPSE (Zucero Therapeutics), was injected intraperitoneally at a dose of 20 mg/kg/week and tumor volume was calculated using the ellipsoid formula: $(\text{width}^2 \times \text{length}) \times {}^1/_2$. The mice were killed when the tumor volume reached 1 cm^3, the tumors weighted, visualized, stained, and photographed with a Zeiss Axio Imager microscope (Carl Zeiss). All animal experiments were pre-approved by the local Ethics Committee for Laboratory Animals in accordance with Swedish legislation.

Intracranial tumor growth, PG545 treatment, and bioluminescent imaging

Using a Hamilton syringe, 1 μL of Gl261/GFP/Luc cells (10^4 cells/μL) was injected stereotactically (1 mm anterior to the bregma, 1.5 mm from the mid-line, and 2.5 mm below the cranial surface) into the brains of NOD-SCID mice and the animals were monitored carefully for signs of tumor for 6 days. Beginning on the seventh day, PG545 (Zucero Therapeutics) was administered intraperitoneally at 20 mg/kg, three times during a period of 12 days. For imaging *in vivo*, 5 mice in each group were anesthetized 8, 48, and 96 hours posttreatment and injected intraperitoneally with luciferin (150 mg/kg), and the intensity of the optical signal detected with an IVIS-CCD camera system (Xenogen) and analyzed with Living Image 2.20 software (Xenogen). Blood, liver, and brain tissues were collected and liver and brain lysates were prepared by using TissueLyser II (Qiagen) according to the manufacturer's protocol. The plasma levels of PG545 was determined by pharmacokinetic sampling/analysis and liver/brain lysates on an API3200 LC-MS/MS, Applied Biosystems, preceded by a Spark Symbiosis Direct On-line Solid Phase Extraction system (19). All animal experiments were pre-approved by the local Ethics Committee for Laboratory Animals in accordance with Swedish legislation.

Indirect immunofluorescent staining of tissue sections

Paraffin-embedded tissue sections were prepared as described (20). The primary antibodies and their dilutions were as follows: anti-mouse CD31 (PECAM-1/Endothelial Cell Marker) rat mAb (1:200 dilution in PBS; Dianova), cleaved caspase-3 (CC3; p-Asp175; 1:100; Cell Signaling Technology), and mouse anti-human Ki-67 antigen mAb (Clone MIB-1; 1:100; DAKO). Ki-67 and CC3 positive cells in tissue sections were scored by the ImageJ Software. As a verification of the automated counting, manual counting of positive nuclei was also performed in a subset of the samples. We found that these two counting methods gave the same result and therefore the figures were based on the Image J results. The threshold for negative staining was placed based on the DAPI color of the nuclei, thus blue nuclei were counted as negative. All other stained nuclei were counted as positive, irrespective of staining intensity. CC3 was determined by nuclear presence. CC3 was found mostly in the nucleus, with an additional few cells per slide displaying weak cytoplasmic presence, but quantification was done solely on the CC3 nuclear staining. For both of these stainings, we analyzed seven images per slide, and in total five tumors per condition.

Collagen invasion assay

Cell spheres were formed in ultra-low attachment plates. Culture media, 0.1 mol/L NaOH, 1 mol/L HEPES, 7.5% sodium bicarbonate and collagen (PureCol; Inamed Biomaterials) were mixed thoroughly following the manufacturer's protocol. Spheres (150–200 μm) were collected individually under a microscope and placed onto collagen using a 100 μL pipette. Finally, gel was added and photographs taken 0, 24, and 48 hours later with a Nikon Eclipse TS 100 microscope (Nikon) and a ZEISS 710 NLO confocal microscope (Carl Zeiss) for two- and three-dimensional visualization, respectively. For PG545 treatment, the inhibitor was added at a final concentration of 50 μg/mL in the complete collagen mixture.

Flow cytometric analysis

For analysis of apoptosis, cells in ice-cold PBS were treated either with 50 μg/mL PG545 or PBS as a negative control or 1 μmol/L staurosporin as a positive control, resuspended in Annexin V binding buffer (10 mmol/L HEPES, 140 mmol/L NaCl, and 2.5 mmol/L $CaCl_2$, pH 7.4), and stained with Annexin V, Alexa Fluor 647 conjugate (Invitrogen) following the manufacturer's protocol. For sorting, cells expressing GFP were selected with the BD AriaIII Cellsorter (BD Biosciences).

Statistical analyses

The data presented are means ± SE, unless otherwise specified in the figure legends. Student unpaired *t* test was used to compare groups. Comparisons of all groups were performed by one-way ANOVA with *post hoc* multiple comparisons. All statistical analyses were performed using the Prism version 6.0 Software (GraphPad).

Results

The levels of HPSE in pediatric brain tumors and tumor cell lines are higher than in the normal brain

Immunohistochemical staining of brain tumor tissue samples of a previously described cohort (21) of CNS-ETs and medulloblastomas revealed higher levels of HPSE than in nonmalignant grey and white matter (Fig. 1A) both in the tumor cells and in the neuropil. Automated quantification revealed the proportion of negative, weak, intermediate, or strong intensity of HPSE staining (Fig. 1B). Medulloblastoma and CNS-ET tumors showed strong positive staining, and to a slighter extent also intermediate staining, but very few areas were classified as negative or weak. Control samples were mostly denoted intermediate, but also showed few areas that were classified as strong. Furthermore, the quantification of negative and weak areas was more prominent in nontumor tissue than in the medulloblastoma and CNS-ET tissue cores. Moreover, Western blot analysis revealed higher expression of HPSE in two medulloblastoma and

Published OnlineFirst July 17, 2017; DOI: 10.1158/1535-7163.MCT-16-0900

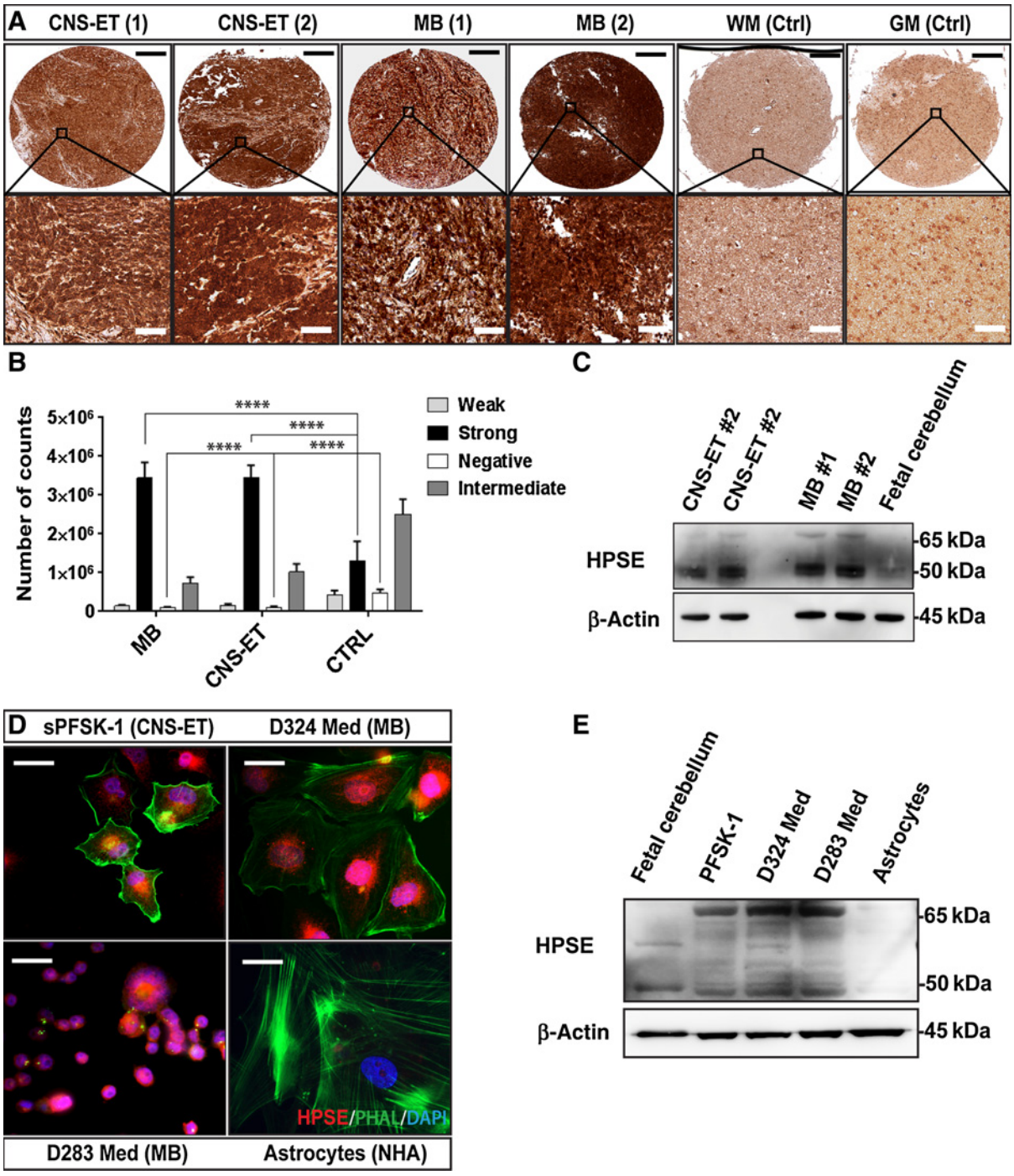

Figure 1.

Expression of HPSE is upregulated in human pediatric CNS embryonal and MB tumors as well as in cell lines derived from such tumors. **A,** Representative staining of a tumor microarray (TMA) of pediatric CNS-ET and medulloblastoma (MB) tumor tissue with anti-HPSE antibody (from left to right, two samples from each tumor type and from normal human brain; WM, white matter; GM, gray matter), Scale bar = 400 μm (top row), 100 μm (bottom row). **B,** Bar graph presenting automated quantification of the TMA; depicting categorization into negative, weak, moderate, and strong staining intensity for HPSE of medulloblastoma and CNS-ET tumors vs. normal (CTRL) brain tissue (groups of four bars for each tissue). Mann–Whitney for individual comparisons and one-way ANOVA with multiple comparisons were performed from the counts among groups (****, $P < 0.0001$). **C,** Western blot analysis showing high levels of HPSE in two CNS-ET and two medulloblastoma surgical specimens compared to fetal cerebellum. β-Actin served as a loading control. **D,** Immunofluorescent staining of PFSK-1, D324, and D283 tumor cells and normal human astrocytes (NHA) for HPSE (red), as well as DAPI staining of nuclei (blue) and F-actin phalloidin filament staining (green). Scale bars = 10 μm. **E,** Western blot analysis showing high levels of HPSE in the PFSK-1, D324, and D283 tumor cell lines compared to low expression in human fetal cerebellum and normal human primary astrocytes. β-Actin served as aloading control.

Published OnlineFirst July 17, 2017; DOI: 10.1158/1535-7163.MCT-16-0900

two CNS-ET cases, compared to fetal cerebellum (Fig. 1C). Analogously, PNET (PFSK-1) and medulloblastoma (D324MB and D283MB) cell lines all displayed greater HPSE immunoreactivity than normal human astrocytes (Fig. 1D). HPSE staining is prominent in the cell nuclei and in perinuclar cytoplasmic granules. Furthermore, Western blotting in lysates from tumor cells readily detected the enzymatically active 50 kDa form, and the latent 65 kDa form of HPSE, whereas normal fetal cerebellum exhibited weaker expression and cultured astrocytes were almost devoid of HPSE (Fig. 1E).

HPSE enhances tumor cell growth

To test whether HPSE can stimulate cell growth, we applied HPSE in two different manners. Either, CM from CHO cells engineered to overexpress enzymatically active 50 kDa HPSE or recombinant, latent 65 kDa HPSE that requires proteolytic cleavage for activation (22) was added to PFSK-1, D283, and D324 cultures. All displayed an increased viable cell count 3 days after treatment with CM (Fig. 2A). The recombinant HPSE led to a small, but significant increase of PFSK-1 and D283 cells over control, with no such effect on D324 cells (Fig. 2B). Hence, exogenous HPSE stimulates tumor cell proliferation, with a more pronounced effect when added as an active form than the pure latent recombinant protein.

HPSE activates the ERK and AKT signaling pathways

To investigate the effect of HPSE on major intracellular signaling pathways associated with proliferation and survival, phosphorylation of ERK and AKT in PNET and medulloblastoma cells treated with rHPSE was examined applying Western blotting. Processing of 65 kDa rHPSE to the 50 kDa form in all the three cell lines was observed after 4 hours, and in PFSK cells to a slight extent even after 1 hour (Fig. 2C, top). With all three cell lines, activation of both ERK and AKT occurred well before processing of HPSE (Fig. 2C). In the case of PFSK-1 and D283 cells, phosphorylation of ERK was detected rapidly after addition of rHPSE and had diminished after 4 hours. In D324 cells, however, an initial ERK activation after 10 minutes was followed by a decline until the end of the experiment (Fig. 2C and D). Regarding AKT activation, PFSK-1 and D283 cells responded with similar rapid kinetics, whereas no obvious activation occurred in the D324 cells (Fig. 2C and E). Clearly, HPSE activated the ERK and AKT pathways rapidly in a manner independent of its enzymatic activity.

Downregulation of HPSE by shRNA attenuates the invasive behavior of PFSK-1 and D324 cells in a manner associated with reduced focal adhesion kinase

Because HS degradation has been implicated in tumor metastasis, a lentivirus shRNA construct was used to reduce the levels of HPSE mRNA by 80% in PFSK and 70% in D324 as verified by qPCR (Fig. 3A). This decreased the area invaded by the cells in a collagen invasion assay by 80% for PFSK-1 and 50% for D324 cells (Fig. 3B and C). Downregulation of HPSE resulted also in attenuated activation of focal adhesion kinase (FAK) in both cell lines (Fig. 3D).

Treatment with the HPSE inhibitor PG545 reduces cell growth *in vitro* and promotes cell death

The involvement of HPSE in PNET and medulloblastoma cell proliferation, invasion, and migration was explored in more detail using PG545, a clinically relevant inhibitor of HPSE (23–25). Proliferation of PFSK-1, D283, and D324 cells, and human primary astrocytes was assessed by the Alamar blue reduction assay. PG545 reduced the growth of PFSK and D283 cells potently in a dose-dependent manner (Fig. 4A), whereas D324 cells were more resistant, with only the highest concentration significantly inhibiting growth, in line with the less pronounced effect of HPSE in these cells (Fig. 2). The growth of primary human astrocytes was not affected by PG545 (Fig. 4A). When PFSK or D283 cells were exposed to CM from cells producing the active form of HPSE, or CM from control cells, simultaneously with PG545, we found that the highest concentration of PG545 reduced cell viability extensively and the CM containing enzymatically active HPSE was not able to counteract this effect (Supplementary Fig. S1A). At a lower concentration of PG545, however, survival was the same for cells treated with PG545 alone, or in combination with CM. Thus, in the presence of PG545, CM with enzymatically active HPSE could not achieve a growth enhancement by HPSE, as that seen in Fig. 2A.

After 48 hours of treatment with PG545, PFSK-1, D283, and D324 cells displayed induction of apoptosis with 63.7%, 35%, and 37.3% Annexin V-positive cells, respectively (Fig. 4B). Thus, apoptotic cell death explains a large proportion of the reduction in cell number caused by PG545. However, in cells that had their HPSE mRNA levels reduced by shRNA against HPSE, we did not detect higher levels of apoptosis (Supplementary Fig. S1B).

Effect of HPSE inhibition on phosphorylation of ERK and AKT

In light of our observations that PG545 reduces cell number and promotes apoptosis, we next investigated the potential influence of this inhibitor on the ERK and AKT signal transduction pathways. Cultures of PFSK-1, D283, and D324 cells were serum starved for 24 hours and then exposed to medium supplemented with 2% FBS with or without PG545, and cell lysates subjected to Western blotting. ERK phosphorylation in PFSK-1 and D324 cells was reduced by PG545, but, inversely, in the case of D283 cells (Fig. 4C; Supplementary Fig. S2A), after an initial reduction, this phosphorylation was elevated following 6 and 24 hours of exposure. At the same time, AKT activation was attenuated by PG545 in all three cell lines at all time-points. HPSE levels were not altered during treatment with PG545 (Supplementary Fig. S2C).

When instead the concentration of PG545 was varied and the cells harvested for Western blotting after 20 hours, only the highest dose (50 μg/mL) stimulated ERK phosphorylation in D283 cells above the control level (Supplementary Fig. S2B). Because the overall effect of this high concentration of the HPSE inhibitor was a dramatic reduction in D283 cell number (Fig. 4A), we conclude that in this case any putative growth-stimulatory effect of ERK phosphorylation was less potent than cell death mechanisms.

PG545 attenuates migration and invasion of PFSK-1 cells

Previous studies implicating HPSE in the motility and dissemination of tumor cells (8, 26) have been performed primarily in models of metastatic cancer, whereas local invasion of pediatric brain tumor cells has not yet been linked to HS degradation. A scratch assay revealed that PG545 attenuated the capacity of PFSK-1 cells to cover the scratched area (Fig. 5A). Moreover, 3D

Published OnlineFirst July 17, 2017; DOI: 10.1158/1535-7163.MCT-16-0900

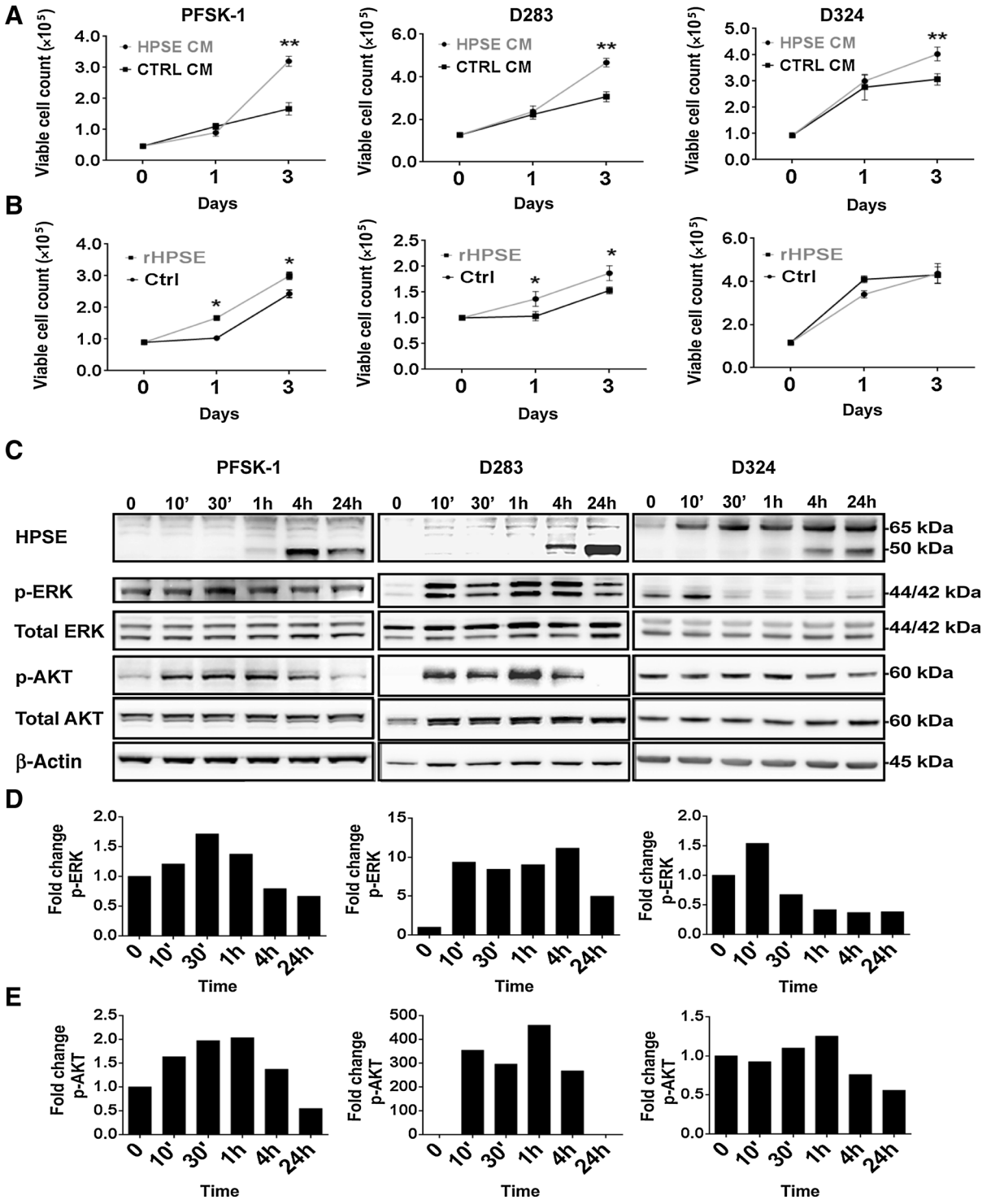

Figure 2.

HPSE enhances tumor cell growth and activates the ERK and AKT signaling pathways. **A,** Proliferation of PFSK-1, D324, and D283 cells was assessed after culturing for 3 days in CM from CHO cells overexpressing HPSE (gray line, 75% CM: 25% fresh medium) or from the corresponding control cells (ctrl, black line; $n = 3$; *, $P < 0.05$; **, $P < 0.01$, as determined by an unpaired t test). **B,** Corresponding growth curves of serum-starved (24 hours) PFSK-1, D324, and (20 h) D283 cells cultured for 3 days in the presence or absence of recombinant HPSE (rHPSE, 1 μg/mL). **C,** Western blotting of full-length (65 kDa) and processed 50-kDa HPSE in PFSK-1, D324, and D283 cells treated with rHPSE (top). Activation of ERK and AKT in serum-starved PFSK-1, D324, and D283 cells after treatment with rHPSE (1 μg/mL). Protein lysates were analyzed for phospho- and total ERK (panels 2 and 3), phospho- and total AKT (panels 4 and 5), and β-actin as a loading control (6th panel). **D** and **E,** The bar graphs depict the densitometric values for activated ERK (**D**) and AKT (**E**) normalized to the total amount of each protein.

Published OnlineFirst July 17, 2017; DOI: 10.1158/1535-7163.MCT-16-0900

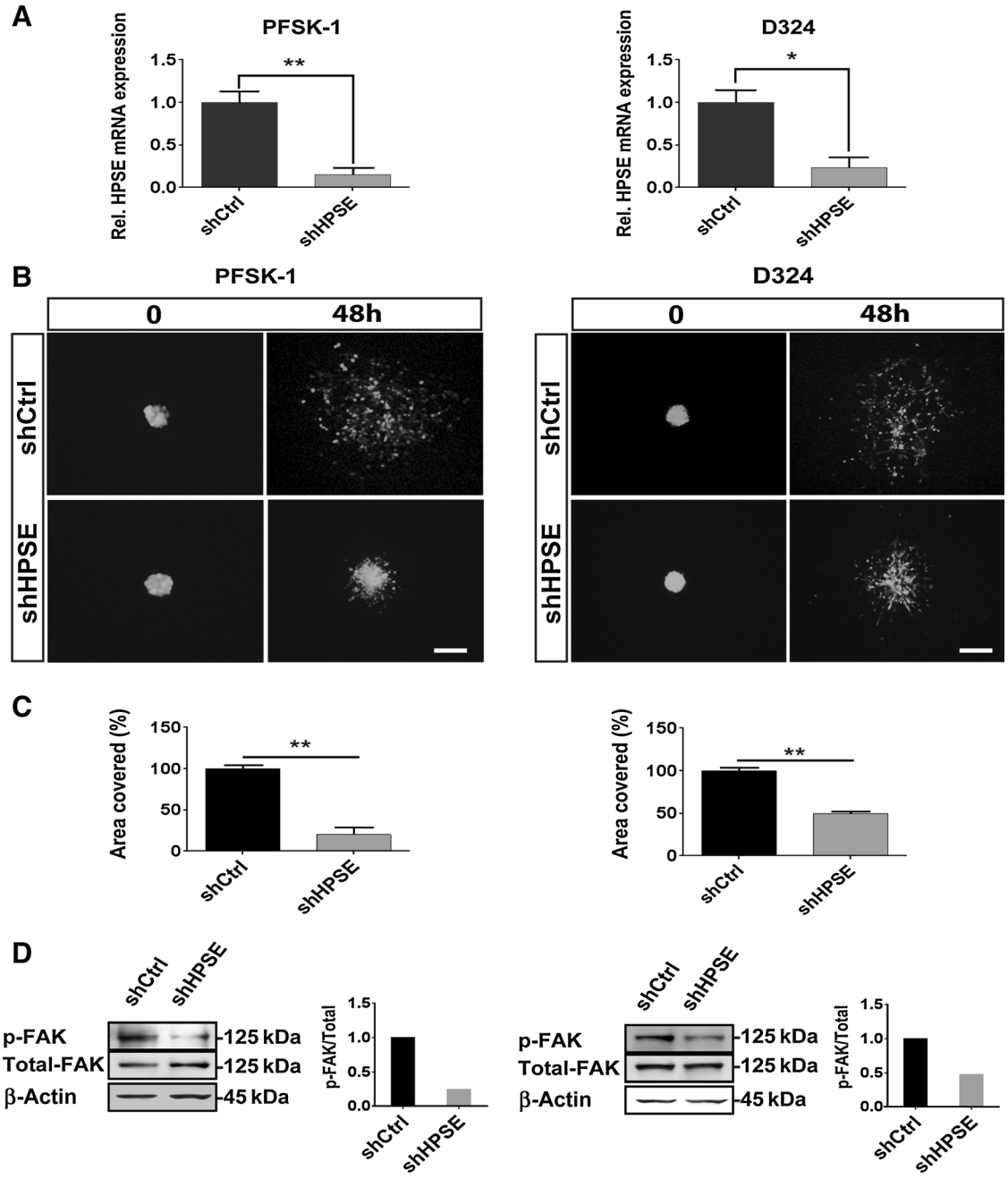

Figure 3.

Downregulation of HPSE by shRNA attenuates the invasive behavior of PFSK-1 and D324 cells concomitant with reduced FAK activation. **A,** Quantitative real-time PCR reveals reduced levels of HPSE mRNA in both PFSK-1 and D324 cells by a lentiviral vector targeting HPSE (shHPSE) in comparison to a control (shCtrl) vector. **B,** Invasion of spheres of PFSK-1 and D324 cells (approximately 200 μm in size), transduced with either shHPSE or shCtrl, into a collagen substrate after 48 hours. GFP-labeled cell spheres were photographed under a Nikon Eclipse TS 100 microscope. Scale bar = 150 μm. **C,** Quantification of the area covered by the cells after 48 hours in collagen ($^{**}P < 0.01$, $n = 12$). **D,** Western blots of FAK phosphorylation in PFSK-1 and D324 cells transduced with either shHPSE or shCtrl. Bar graphs presenting the densitometric values for activation normalized to the total amount of each protein are shown for the respective western blots. β-Actin served as a loading control.

visualization of a collagen gel invasion assay also showed a significant reduction in invasiveness (Fig. 5B). Western blotting analysis of phosphorylated SRC (Tyr4167; Fig. 5C) and FAK (Tyr397; Fig. 5D) demonstrated that activation of both factors was blocked by PG545 in a dose-dependent manner.

PG545 inhibits the growth of tumors produced *in vivo* by PFSK-1 or D283 cells

Because PG545 was found not to pass the blood–brain barrier (Supplementary Fig. S3A), PFSK-1 and D283 cells were injected subcutaneously into the flanks of NOD-SCID mice and after

Published OnlineFirst July 17, 2017; DOI: 10.1158/1535-7163.MCT-16-0900

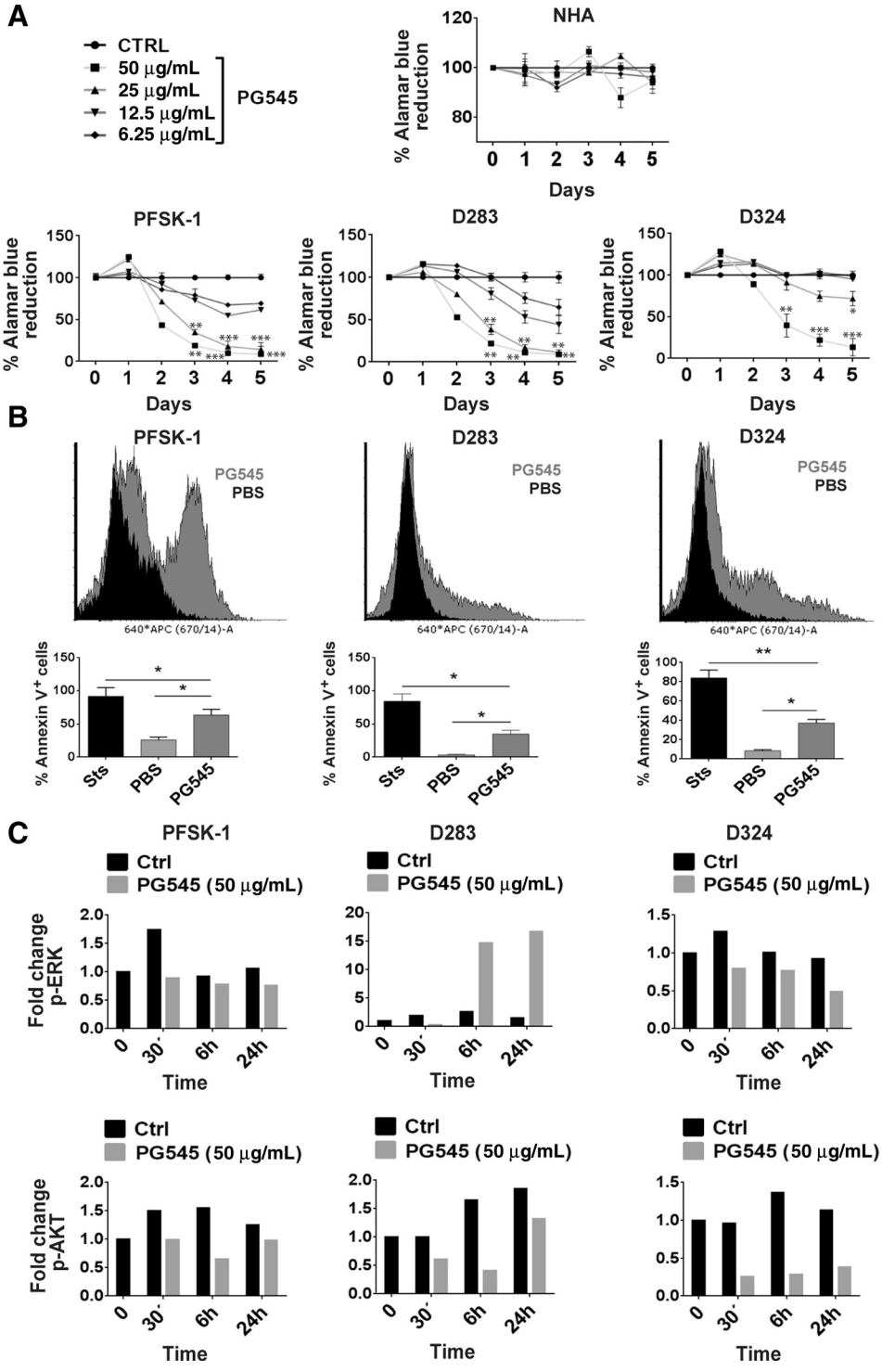

Figure 4.

Treatment with the HPSE inhibitor PG545 reduces cell growth *in vitro*, promotes cell death, and alters the ERK and AKT signaling pathways. **A,** Alamar blue reduction by PFSK-1, D324, and D283 cells and human normal astrocytes (NHA) was monitored for 5 days in the presence of PG545 ($n = 3$, **, $P < 0.01$; ***, $P < 0.001$). Analysis of the growth curves at different time-points and doses was done by two-way ANOVA and the PG545 and vehicle-treated values were compared employing a two-tailed unpaired *t* test. **B,** Flow cytometric histograms of Annexin V labeling of PFSK-1, D324, and D283 cells treated with 50 μg/mL PG545, PBS (as negative control) or 1 μmol/L staurosporin (sts) as positive control for 48 hours. The quantification graphs depict the percentages of Annexin-V positive cells ($n = 3$, *, $P < 0.05$; **, $P < 0.01$; ***, $P < 0.001$) as determined by two-way ANOVA analysis. **C,** Quantification of Western blots of ERK and AKT activation normalized to the total amount of each protein in serum-stimulated PFSK-1, D324, and D283 cells treated with PG545 (50 μg/mL) or PBS (ctrl).

tumors had formed, PG545 was injected intraperitoneally and the tumor size subsequently monitored. The growth of both PFSK-1 and D283 tumors was slower already after 3 days of PG545 treatment (Fig. 6A), by the end of the experiment there was a marked reduction in tumor volume (85.3% and 88.6%, respectively) and weight (3- and 5-fold, respectively; Supplementary Fig. S3B). Repeated administration of PG545 for 14 days did not cause any overt side effects such as weight loss of the mice (Supplementary Fig. S3C).

Inhibition of HPSE attenuated the proliferation and promoted apoptosis of tumor cells *in vivo*

To investigate the mechanism(s) by which PG545 acts on tumor cells in further detail, histologic sections were stained for

Published OnlineFirst July 17, 2017; DOI: 10.1158/1535-7163.MCT-16-0900

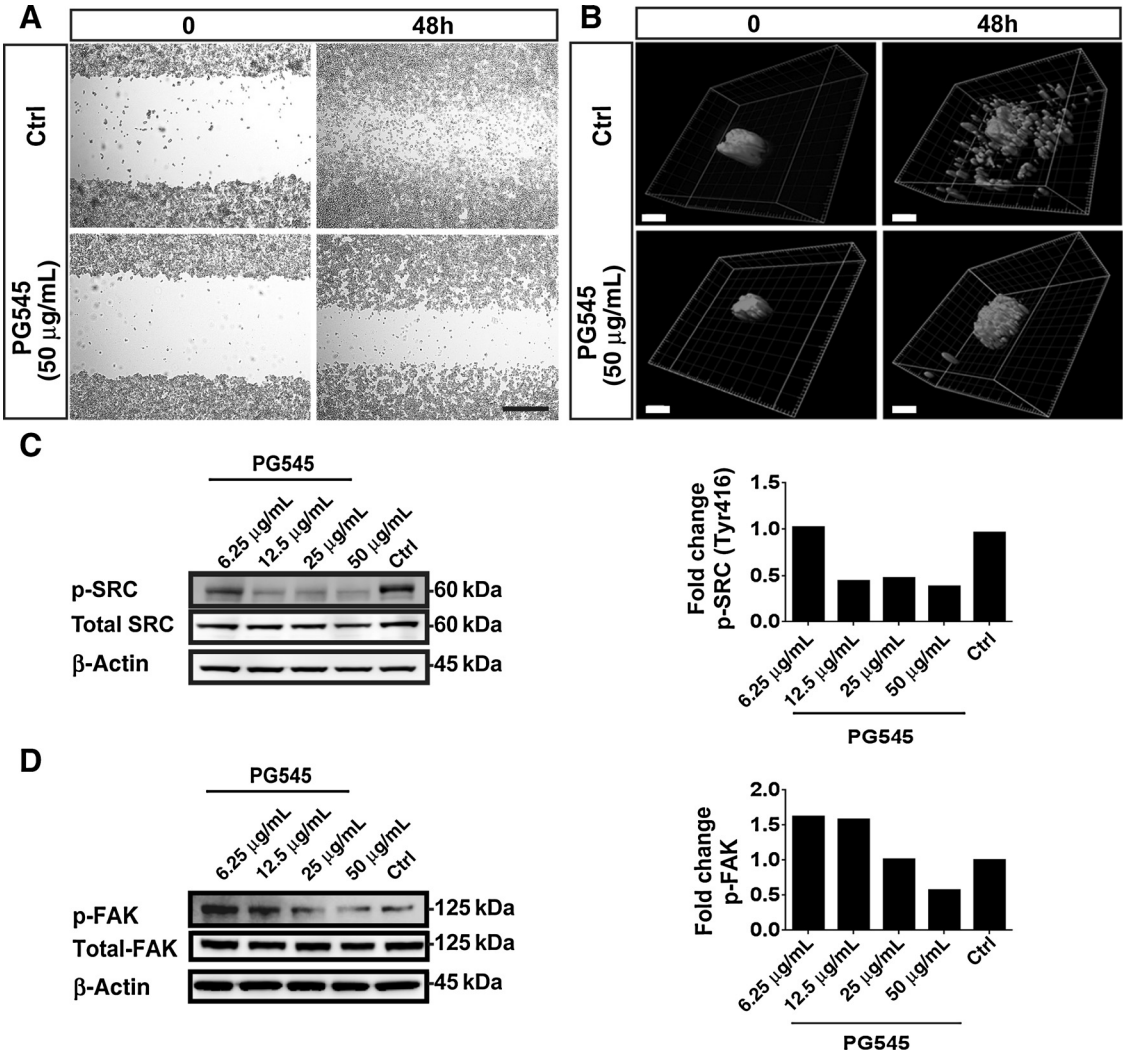

Figure 5.

PG545 attenuates the migration and invasion of PFSK-1 cells. **A,** Scratch assay of the PFSK-1 cell line 48 hours after addition of 50 μg/mL PG545 or PBS (ctrl) reveals that the inhibitor attenuated the capacity of the cells to cover the scratched area. **B,** Invasion of approximately 200 μm spheres of PFSK-1 cells into a collagen matrix 48 hours after addition of 50 μg/mL PG545 or PBS (ctrl). Scale bars = 100 μm. **C** (Left), Western blots showing SRC phosphorylation in PFSK-1 cells treated with various concentrations of PG545 for 20 hours. β-Actin served as a loading control. (Right) Bar graphs representing the densitometric values for SRC activation normalized to the total amount of SRC protein. **D** (Left)**,** Western blots showing FAK phosphorylation in PFSK-1 cells treated with various concentrations of PG545 for 20 hours. β-Actin served as a loading control. (Right) Bar graphs representing the densitometric values for FAK activation normalized to the total amount of FAK protein.

Ki-67 to assess cell proliferation in xenograft tumors. The number of positive cells was reduced approximately 50% by PG545 in both types of tumors (Fig. 6B), consistent with our *in vitro* findings that inhibition of HPSE induces cell death (Fig. 4B). The number of cells stained for CC3, a marker for apoptosis, rose 10-fold in PFSK-1 and 5-fold in D283 tumors upon treatment with PG545 (Fig. 6C).

PG545 inhibits vascularization in pediatric brain tumor xenografts

When tumor vessels were immuno-stained for CD31, the total area stained relative to the area of all cell nuclei stained blue by DAPI fell seven- and nine-fold in PFSK-1 and D283 tumors in response to treatment with PG545, respectively (Fig. 6D, top bar graphs). PG545 reduced the average vessel diameter four- and six-fold in PFSK-1 and D283 tumors, respectively (Fig. 6D, bottom bar graphs). Clearly, PG545 inhibits tumor neovascularization. Moreover, histologic examination revealed less bleeding in PG545-treated tumors, suggesting vessel normalization (Supplementary Fig. S3D).

Discussion

Several malignant brain tumors, including medulloblastomas and other pediatric embryonal tumors, are invasive and thereby particularly aggressive, but no current clinical treatments specifically and effectively target the brain tumor microenvironment. We report here that HPSE is associated with concomitant activation of mitogenic and survival signaling pathways, by stimulating

Published OnlineFirst July 17, 2017; DOI: 10.1158/1535-7163.MCT-16-0900

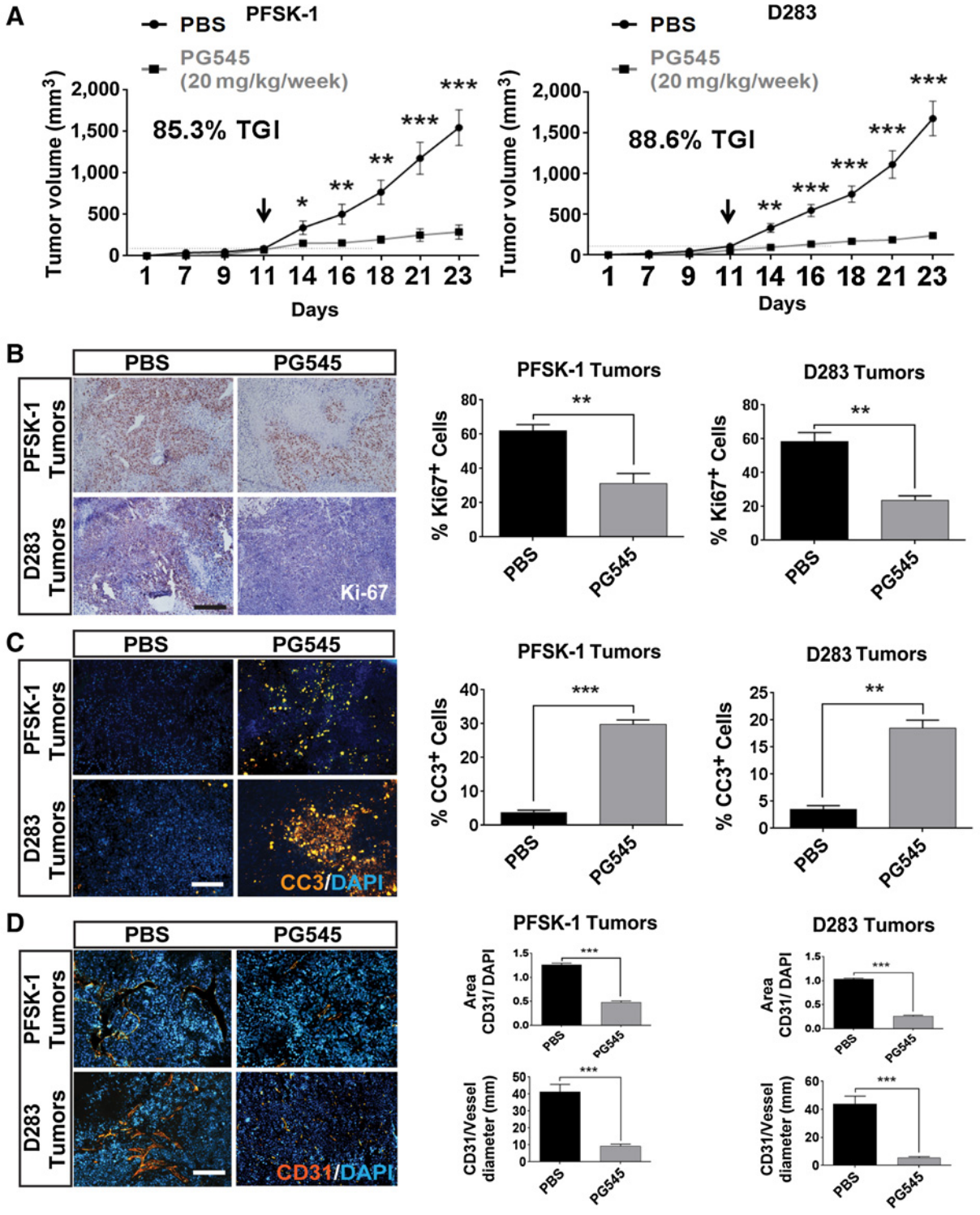

Figure 6.

PG545 inhibits tumor growth, promotes apoptosis, and reduces tumor vascularization *in vivo*. **A,** Growth of subcutaneous PFSK-1 and D283 tumors in mice treated by intraperitoneal administration of PG545 (grey line) or vehicle (PBS; black line; $n = 11$ mice/group; *, $P < 0.05$; **, $P < 0.01$; ***, $P < 0.001$). By day 14, tumor growth inhibition (TGI) was 85.3% and 88.6%, respectively. **B,** Staining of tumors for Ki-67 with quantification bar graphs shown on the right. **, $P < 0.01$. **C,** Staining for CC3 with quantification graphs are shown on the right. **, $P < 0.01$; ***, $P < 0.001$. **D,** Staining for CD31 reveals reduced vascularization of PG545-treated tumors. Quantification of the diameter of CD31 positive vessels and total area per cell staining for CD31 are displayed on the right ($n = 5$ tumors/group; *, $P < 0.05$; **, $P < 0.01$; ***, $P < 0.001$). Scale bar = 100 μm.

Published OnlineFirst July 17, 2017; DOI: 10.1158/1535-7163.MCT-16-0900

the growth and invasion of pediatric brain tumor cells both *in vitro* and *in vivo*.

Although, the importance of HSPGs has been emphasized in several studies concerning cancer and regeneration (11, 27–32), their role in connection with pediatric brain tumors remains poorly understood. Our present findings that the level of HPSE is elevated in cases of medulloblastoma and CNS-embryonal tumors in comparison to normal white and gray matter and cultured astrocytes, indicate that this enzyme could be a specific drug target. Our own recent results suggest that specific degradation of matrix HS contributes to the progression of glioma (7) and here we establish that pediatric tumor cells might circumvent regulatory circuits by upregulating HPSE.

Cleavage of the HS side chains of HSPGs by HPSE activity or some function of the latent form of HPSE (22) has been correlated to metastasis by cancer cells (33) but usually not directly correlated to cell proliferation. Nonetheless, it is well established that HSPGs act as co-receptors for growth factors and cytokines and potentiate their activation (34). Although HPSE stimulates tumor growth in a variety of systems, there is little evidence to date that this enzyme is mitogenic, although we recently reported such an effect on adult brain tumor cells (7).

It is becoming increasingly clear that in addition to its enzymatic activity, HPSE has nonenzymatic functions (16, 35) that are still incompletely understood. The notion that latent HPSE activates ERK in multiple myeloma (36) is in agreement with our finding that rapid activation of both the ERK and AKT signaling pathways in tumor cells occurred well before proteolytic processing of pro-HPSE to its active, 50 kDa form.

We also observed that downregulation of HPSE expression by shRNA blocks the invasion of tumor cells into a model collagen matrix. In light of the great abundance of proteoglycans in brain ECM, this suggests that inhibition of HPSE could diminish the matrix remodeling that favors invasion by medulloblastoma and PNET cells. Indeed, tumor cell invasiveness is also reduced after knockdown of HPSE in myeloma and melanoma cells (37, 38) and as shown here, lowering HPSE levels attenuates phosphorylation of FAK, a key regulator of cancer cell invasion. FAK has previously been shown to be a downstream target of HPSE (16, 39), but to our knowledge we provide the first demonstration of the involvement of the HPSE–FAK axis in invasion by brain cancer cells.

Having shown that HPSE plays a role in the growth of pediatric brain tumor cells, activation of intracellular signaling pathways and cell invasion, we reasoned that because cancer cells lose their tumorigenic/metastatic abilities following HPSE gene silencing (25), it might be therapeutically beneficial to block HPSE activity with the clinically relevant HPSE inhibitor PG545 (25). PG545 efficiently reduced tumor cell numbers in a dose-dependent manner, largely by decreasing proliferation and promoting apoptosis, without affecting primary human astrocytes, even at the highest concentrations tested. In line with this, the AKT signal transduction pathway that promotes survival was decreased upon PG545 treatment of all the tumor cell lines. Because progression of these types of tumor involves local invasion and the migrating cancer cells often evade current chemotherapies, it was encouraging to find that matrix degradation and cell spread were also blocked by PG545, with a concomitant reduction in the phosphorylation of FAK and SRC, critical mediators of tumor cell invasion (40–42).

PG545 inhibits growth and metastasis in several models of solid cancer including pancreatic, lung, hepatocellular, colon, melanoma, and head/neck tumors (19, 24). Importantly, here PG545 inhibited the growth of xenografted PFSK and D283 tumors in mice by 85% to 88%, that is, more than in the case of breast carcinoma (50% TGI; ref. 23) and GBM (59% to 69% TGI; ref. 7), and the reduction we observed was correlated with significant antiproliferative, anti-angiogenic, and pro-apoptotic properties. Moreover, PG545 was well tolerated, with no loss of body weight during the 12 days of treatment, suggesting that targeting HPSE should not cause overt adverse side effects.

Although PG545 efficiently penetrates into solid tumors (19), its capacity to cross the blood–brain barrier had not previously been investigated. Because of its size (2363.8 kDa) our finding that this inhibitor failed to pass the BBB was not surprising. This means, however, that treating brain tumors with PG545 to block HPSE will require direct injections into the brain, or intrathecal administration to the cerebrospinal fluid. Regardless of these challenges, we propose that targeting HPSE should be evaluated further as a novel treatment for malignant pediatric brain tumors, such as medulloblastoma and other embryonal tumors.

Disclosure of Potential Conflicts of Interest

K. Dredge and E. Hammond are full time employees of Zucero Therapeutics. No potential conflicts of interest were disclosed by the other authors.

Authors' Contributions

Conception and design: A. Spyrou, S. Kundu, T. Olofsson, K. Forsberg-Nilsson
Development of methodology: A. Spyrou, S. Kundu, T. Olofsson, K. Dredge
Acquisition of data (provided animals, acquired and managed patients, provided facilities, etc.): A. Spyrou, L. Haseeb, T. Olofsson, U. Barash
Analysis and interpretation of data (e.g., statistical analysis, biostatistics, computational analysis): A. Spyrou, E. Hammond, I. Vlodavsky, K. Forsberg-Nilsson
Writing, review, and/or revision of the manuscript: A. Spyrou, L. Haseeb, T. Olofsson, K. Dredge, E. Hammond, I. Vlodavsky, K. Forsberg-Nilsson
Administrative, technical, or material support (i.e., reporting or organizing data, constructing databases): A. Spyrou, D. Yu, K. Dredge, E. Hammond, U. Barash
Study supervision: K. Forsberg-Nilsson

Acknowledgments

We wish to thank Mrs A. Hermansson for excellent technical assistance and the personnel at the Animal Facility for animal care. Imaging was performed with the support of the Science for Life Lab BioVis Platform, Uppsala, and the authors especially thank Dr. Mathias Molnar for assistance with microscopy and Dr. Dirk Pacholsky for FACS cell sorting. We extend our gratitude also to Linda Wright at TetraQ, University of Queensland, for measuring PG545 in mouse samples.

Grant Support

This study was supported by the following grants to K. Forsberg-Nilsson: the Swedish Cancer Society (No. 130500), Swedish Research Council (No. 521-2013-3356), the Swedish Childhood Cancer Foundation (Nos. PROJ12/093 and NCp2015-0077), and grants to Argyris Spyrou from the Swedish Childhood Cancer Foundation and Bergmark and Enestrom Foundations. This project has also received funding from the European Union's Horizon 2020 research and innovation programme under the Marie Skøodowska-Curie grant agreement No. 645756. I. Vlodavsky is a research Professor of the Israel Cancer Research Fund (ICRF).

The costs of publication of this article were defrayed in part by the payment of page charges. This article must therefore be hereby marked *advertisement* in accordance with 18 U.S.C. Section 1734 solely to indicate this fact.

Received December 22, 2016; revised April 30, 2017; accepted May 22, 2017; published OnlineFirst July 17, 2017.

Published OnlineFirst July 17, 2017; DOI: 10.1158/1535-7163.MCT-16-0900

References

1. Louis DN, Perry A, Reifenberger G, von Deimling A, Figarella-Branger D, Cavenee WK, et al. The 2016 World Health Organization Classification of Tumors of the Central Nervous System: a summary. Acta Neuropathol 2016;131:803–20.
2. Ohba S, Yoshida K, Hirose Y, Ikeda E, Kawase T. A supratentorial primitive neuroectodermal tumor in an adult: a case report and review of the literature. J Neurooncol 2008;86:217–24.
3. Sturm D, Orr BA, Toprak UH, Hovestadt V, Jones DT, Capper D, et al. New brain tumor entities emerge from molecular classification of CNS-PNETs. Cell 2016;164:1060–72.
4. Cheng JC, Chou CH, Kuo ML, Hsieh CY. Radiation-enhanced hepatocellular carcinoma cell invasion with MMP-9 expression through PI3K/Akt/NF-kappaB signal transduction pathway. Oncogene 2006;25:7009–18.
5. Steck PA, Moser RP, Bruner JM, Liang L, Freidman AN, Hwang TL, et al. Altered expression and distribution of heparan sulfate proteoglycans in human gliomas. Cancer Res 1989;49:2096–103.
6. Phillips JJ, Huillard E, Robinson AE, Ward A, Lum DH, Polley M-Y, et al. Heparan sulfate sulfatase SULF2 regulates PDGFRα signaling and growth in human and mouse malignant glioma. J Clin Invest 2012;122:911–22.
7. Kundu S, Xiong A, Spyrou A, Wicher G, Marinescu VD, Edqvist PD, et al. Heparanase promotes glioma progression and is inversely correlated with patient survival. Mol Cancer Res 2016;14:1243–53.
8. Vlodavsky I, Goldshmidt O. Properties and function of heparanase in cancer metastasis and angiogenesis. Haemostasis 2001;31Suppl 1:60–3.
9. Fux L, Ilan N, Sanderson RD, Vlodavsky I. Heparanase: busy at the cell surface. Trends Biochem Sci 2009;34:511–9.
10. Ilan N, Elkin M, Vlodavsky I. Regulation, function and clinical significance of heparanase in cancer metastasis and angiogenesis. Int J Biochem Cell Biol 2006;38:2018–39.
11. Simizu S, Ishida K, Osada H. Heparanase as a molecular target of cancer chemotherapy. Cancer Sci 2004;95:553–8.
12. Trojanowski JQ, Friedman HS, Burger PC, Bigner DD. A rapidly dividing human medulloblastoma cell line (D283 MED) expresses all three neurofilament subunits. Am J Pathol 1987;126:358–63.
13. Zetser A, Levy-Adam F, Kaplan V, Gingis-Velitski S, Bashenko Y, Schubert S, et al. Processing and activation of latent heparanase occurs in lysosomes. J Cell Sci 2004;117(Pt 11):2249–58.
14. Xie Y, Bergstrom T, Jiang Y, Johansson P, Marinescu VD, Lindberg N, et al. The human glioblastoma cell culture resource: validated cell models representing all molecular subtypes. EBioMedicine 2015;2:1351–63.
15. Zetser A, Bashenko Y, Miao HQ, Vlodavsky I, Ilan N. Heparanase affects adhesive and tumorigenic potential of human glioma cells. Cancer Res 2003;63:7733–41.
16. Riaz A, Ilan N, Vlodavsky I, Li JP, Johansson S. Characterization of heparanase-induced phosphatidylinositol 3-kinase-AKT activation and its integrin dependence. J Biol Chem 2013;288:12366–75.
17. Jin C, Yu D, Hillerdal V, Wallgren A, Karlsson-Parra A, Essand M. Allogeneic lymphocyte-licensed DCs expand T cells with improved antitumor activity and resistance to oxidative stress and immunosuppressive factors. Mol Ther Methods Clin Dev 2014;1:14001.
18. Ferro V, Liu L, Johnstone KD, Wimmer N, Karoli T, Handley P, et al. Discovery of PG545: a highly potent and simultaneous inhibitor of angiogenesis, tumor growth, and metastasis. J Med Chem 2012;55:3804–13.
19. Dredge K, Hammond E, Handley P, Gonda TJ, Smith MT, Vincent C, et al. PG545, a dual heparanase and angiogenesis inhibitor, induces potent anti-tumour and anti-metastatic efficacy in preclinical models. Br J Cancer 2011;104:635–42.
20. Bergstrom T, Holmqvist K, Tararuk T, Johansson S, Forsberg-Nilsson K. Developmentally regulated collagen/integrin interactions confer adhesive properties to early postnatal neural stem cells. Biochim Biophys Acta 2014;1840:2526–32.
21. Polajeva J, Bergstrom T, Edqvist PH, Lundequist A, Sjosten A, Nilsson G, et al. Glioma-derived macrophage migration inhibitory factor (MIF) promotes mast cell recruitment in a STAT5-dependent manner. Mol Oncol 2014;8:50–8.
22. Goldshmidt O, Zcharia E, Cohen M, Aingorn H, Cohen I, Nadav L, et al. Heparanase mediates cell adhesion independent of its enzymatic activity. FASEB J 2003;17:1015–25.
23. Dredge K, Hammond E, Davis K, Li CP, Liu L, Johnstone K, et al. The PG500 series: novel heparan sulfate mimetics as potent angiogenesis and heparanase inhibitors for cancer therapy. Invest New Drugs 2010;28:276–83.
24. Hammond E, Brandt R, Dredge K. PG545, a heparan sulfate mimetic, reduces heparanase expression *in vivo*, blocks spontaneous metastases and enhances overall survival in the 4T1 breast carcinoma model. PLoS One 2012;7:e52175.
25. Rivara S, Milazzo FM, Giannini G. Heparanase: a rainbow pharmacological target associated to multiple pathologies including rare diseases. Future Med Chem 2016;8:647–80.
26. Meirovitz A, Hermano E, Lerner I, Zcharia E, Pisano C, Peretz T, et al. Role of heparanase in radiation-enhanced invasiveness of pancreatic carcinoma. Cancer Res 2011;71:2772–80.
27. Blackhall FH, Merry CL, Davies EJ, Jayson GC. Heparan sulfate proteoglycans and cancer. Br J Cancer 2001;85:1094–8.
28. Cohen E, Doweck I, Naroditsky I, Ben-Izhak O, Kremer R, Best LA, et al. Heparanase is overexpressed in lung cancer and correlates inversely with patient survival. Cancer 2008;113:1004–11.
29. Forsberg M, Holmborn K, Kundu S, Dagalv A, Kjellen L, Forsberg-Nilsson K. Undersulfation of heparan sulfate restricts differentiation potential of mouse embryonic stem cells. J Biol Chem 2012;287:10853–62.
30. Kim AW, Xu X, Hollinger EF, Gattuso P, Godellas CV, Prinz RA. Human heparanase-1 gene expression in pancreatic adenocarcinoma. J Gastrointest Surg 2002;6:167–72.
31. Lim HC, Multhaupt HA, Couchman JR. Cell surface heparan sulfate proteoglycans control adhesion and invasion of breast carcinoma cells. Mol Cancer 2015;14:15.
32. Okolicsanyi RK, Griffiths LR, Haupt LM. Mesenchymal stem cells, neural lineage potential, heparan sulfate proteoglycans and the matrix. Dev Biol 2014;388:1–10.
33. Goldshmidt O, Zcharia E, Abramovitch R, Metzger S, Aingorn H, Friedmann Y, et al. Cell surface expression and secretion of heparanase markedly promote tumor angiogenesis and metastasis. Proc Natl Acad Sci U S A 2002;99:10031–6.
34. Sarrazin S, Lamanna WC, Esko JD. Heparan sulfate proteoglycans. Cold Spring Harb Perspect Biol 2011;3:1–33.
35. Katz BZ, Muhl L, Zwang E, Ilan N, Herishanu Y, Deutsch V, et al. Heparanase modulates heparinoids anticoagulant activities via non-enzymatic mechanisms. Thromb Haemost 2007;98:1193–9.
36. Purushothaman A, Chen L, Yang Y, Sanderson RD. Heparanase stimulation of protease expression implicates it as a master regulator of the aggressive tumor phenotype in myeloma. J Biol Chem 2008;283:32628–36.
37. Liu X, Fang H, Chen H, Jiang X, Fang D, Wang Y, et al. An artificial miRNA against HPSE suppresses melanoma invasion properties, correlating with a down-regulation of chemokines and MAPK phosphorylation. PLoS One 2012;7:e38659.
38. Reiland J, Kempf D, Roy M, Denkins Y, Marchetti D. FGF2 binding, signaling, and angiogenesis are modulated by heparanase in metastatic melanoma cells. Neoplasia 2006;8:596–606.
39. Ma XM, Shen ZH, Liu ZY, Wang F, Hai L, Gao LT, et al. Heparanase promotes human gastric cancer cells migration and invasion by increasing Src and p38 phosphorylation expression. Int J Clin Exp Pathol 2014;7:5609–21.
40. Hsia DA, Mitra SK, Hauck CR, Streblow DN, Nelson JA, Ilic D, et al. Differential regulation of cell motility and invasion by FAK. J Cell Biol 2003;160:753–67.
41. Liu XG, Guo Y, Yan ZQ, Guo MY, Zhang ZG, Guo CA. [FAK/c-Src signaling pathway mediates the expression of cell surface HSP90 in cultured human prostate cancer cells and its association with their invasive capability]. Zhonghua Zhong Liu Za Zhi 2011;33:340–4.
42. Megison ML, Stewart JE, Nabers HC, Gillory LA, Beierle EA. FAK inhibition decreases cell invasion, migration and metastasis in MYCN amplified neuroblastoma. Clin Exp Metastasis 2013;30:555–68.

Published OnlineFirst July 17, 2017; DOI: 10.1158/1535-7163.MCT-16-0900

Molecular Cancer Therapeutics

Inhibition of Heparanase in Pediatric Brain Tumor Cells Attenuates their Proliferation, Invasive Capacity, and *In Vivo* Tumor Growth

Argyris Spyrou, Soumi Kundu, Lulu Haseeb, et al.

Mol Cancer Ther Published OnlineFirst July 17, 2017.